Trellis-Coded Pulse-Position Modulation for Indoor Wireless Infrared Communications

David C. M. Lee, *Student Member, IEEE*, Joseph M. Kahn, *Member, IEEE,* and Malik D. Audeh, *Member, IEEE*

Abstract— We analyze the performance of trellis-coded pulse-position modulation (PPM) on indoor, wireless infrared channels. We show that maximum-likelihood sequence detection (MLSD) of trellis-coded PPM is very effective in mitigating the multipath dispersion on such channels. We present code search results for high constraint-length, rate-2/3, 8-PPM and rate-3/4, 16-PPM codes. We provide bit-error rate curves and intersymbol interference power-penalties for MLSD of PPM with these codes, evaluated on ceiling-bounce channel models with delay spread per bit duration ratios of 0.01–0.3. Finally, we present Monte Carlo simulation results to verify our analysis.

Index Terms—Pulse-position modulation, trellis-coded modulation, wireless infrared communications.

I. INTRODUCTION

THE enormous growth of personal computers and portable communication terminals has generated strong interest in high-speed wireless links for the interconnection of portable devices and for the establishment of local-area networks (LAN's) [1]–[3]. For wide applicability, a wireless link should be compact, consume little power, and be easy to align, yet be robust against background noise and interference from other users. As a transmission medium for indoor wireless communication, infrared has several advantages over radio, such as an enormous unregulated bandwidth and the absence of interference between links operating in rooms separated by walls or other opaque barriers [2].

Indoor infrared links, however, must operate in the presence of strong ambient radiation from sunlight, incandescent lighting, and fluorescent lighting, which induces shot noise and cyclostationary noise in the receiver photodiode. Concerns of eye safety and power consumption limit the average transmitter power, further restricting the operating range. While infrared does not suffer from multipath fading, reflections from walls, floor, and room objects cause multipath dispersion, resulting in intersymbol interference (ISI). This effect is particularly pronounced in links using nondirectional transmitters and/or receivers that operate at bit rates above 10 Mbits/s [2].

Pulse-position modulation (PPM) [3] offers high average-power efficiency, but due to its poor bandwidth efficiency, it is more susceptible to multipath-induced ISI than simple on–off keying (OOK). Audeh *et al.* [4] showed that maximum-likelihood sequence detection (MLSD) of uncoded PPM links on measured indoor wireless infrared channels at 10–30 Mbits/s provides significant improvements in average-power efficiency over OOK. However, they found that even with MLSD, uncoded PPM suffers larger ISI penalties than OOK. Previous work on coding with PPM [5], [6] has focused on the free-space, direct-detection, optical channel, in which there is typically little ISI. In previous work, we have applied simple, rate-2/3 codes with 8-PPM on the measured channels in [7], showing that trellis-coded PPM is very effective in mitigating the multipath ISI [8].

In this paper, we evaluate the use of trellis-coded PPM on multipath infrared channels. First, we describe the channel and noise models for the wireless indoor infrared channel. Then we describe MLSD of trellis-coded PPM. We use the code search technique of [10] to find good rate-2/3 codes for 8-PPM and rate-3/4 codes for 16-PPM. We compare the results with those for MLSD of uncoded 16-PPM and 32-PPM, which have comparable bandwidth requirements and receiver complexity. The results indicate that trellis-coded 16-PPM provides the best average-power efficiency among the modulation techniques considered.

II. CHANNEL AND NOISE MODELS

In order to obtain a high SNR, practical nondirected systems employing intensity modulation with direct detection (IM/DD) use photodetectors having large areas, on the order of 0.01–1 cm^2, or 10^6–10^8 square wavelengths, which result in optically incoherent reception without multipath fading. In intensity modulation, the transmitted signal $X(t)$ is instantaneous optical power. The received signal $Z(t)$ is the detector photocurrent, which is the responsivity R multiplied by the optical power integrated over the detector surface. The multipath dispersion resulting from reflections off walls, floor, and room objects can be described by an LTI impulse response $h(t)$ that changes significantly only when the transmitter, receiver, or intervening reflectors are moved by distances on the order of centimeters [2]. We use the ceiling-bounce functional model [11] for the channel impulse response, as described in Section IV.

The optical IM/DD channel is normally modeled by a signal-dependent, Poisson-rate, photon-counting model. Due
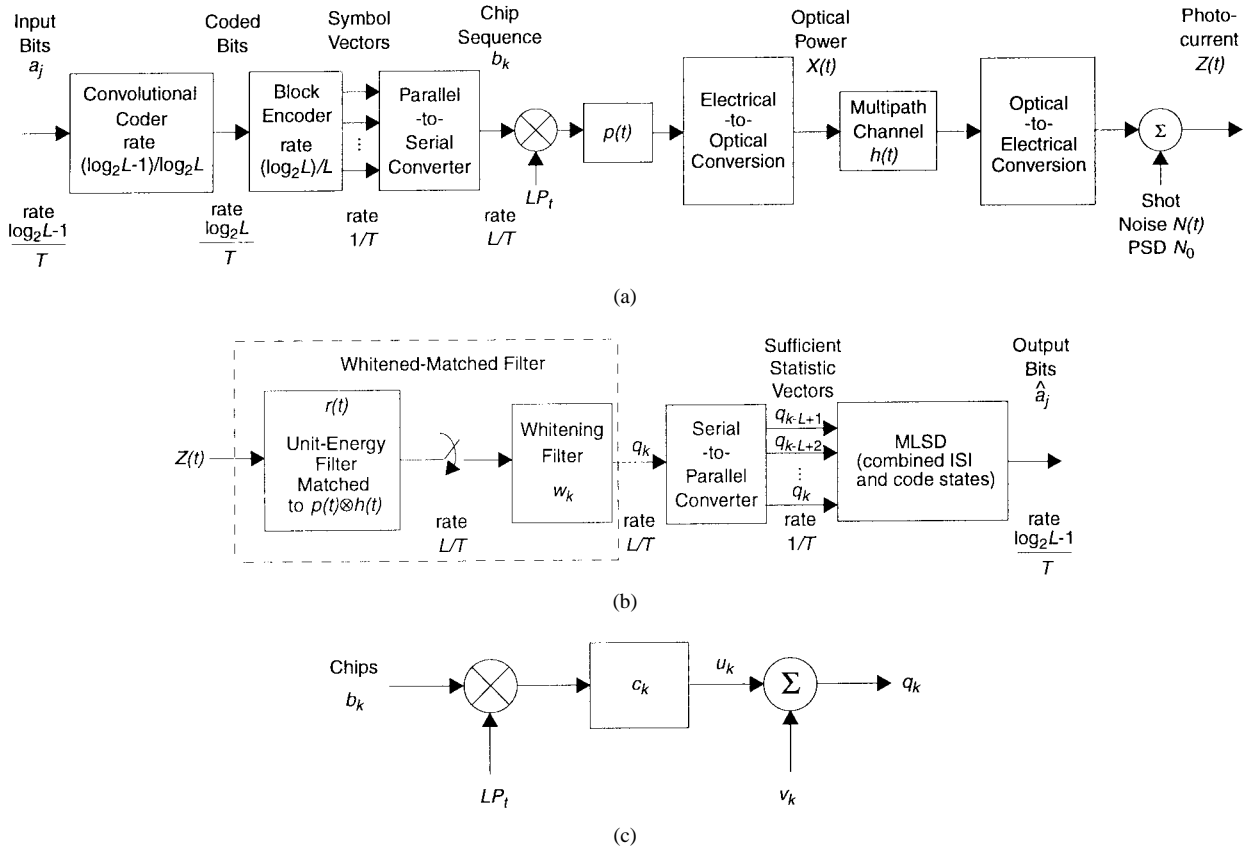
(a)

(b)

(c)

Fig. 1. Trellis-coded L-PPM system block diagram. (a) Block diagram of trellis-coded L-PPM transmission over a multipath channel. The electrical signal $Z(t)$ is the input to the receiver. (b) Block diagram of trellis-coded L-PPM receiver with whitened-matched filter followed by MLSD of combined ISI and trellis code. (c) Discrete-equivalent model of L-PPM system, prior to MLSD, sampled at the chip rate L/T.

to the intense ambient light in indoor environments, a wireless indoor infrared channel corresponds to the background light-limited, high-photon-rate case. The intense ambient light that distinguishes this environment from optical fiber and free-space optical systems leads to certain simplifications in the photon-counting model [3].

The channel model for a nondirected IM/DD infrared link can be summarized in a simple form:

$$Z(t) = RX(t) \otimes h(t) + N(t). \quad (1)$$

The received photocurrent $Z(t)$ is the convolution of the transmitted optical power $X(t)$ with a channel impulse response $h(t)$ (fixed for a given configuration of transmitter, receiver, and intervening reflectors), scaled by the photodetector responsivity R, plus an additive noise $N(t)$, which is usually modeled as white, Gaussian, and independent of $X(t)$ [3].

The channel model described by (1) is similar to a conventional linear, baseband channel. In particular, the receiver electrical signal-to-noise ratio (SNR) is proportional to $|X(t)|^2$, as in conventional electrical and radio systems. However, the average transmitted power constraint for an IM/DD infrared link [3] is given by

$$P_t = \lim_{T \to \infty} \frac{1}{2T} \int_{-T}^{T} X(t)\,dt. \quad (2)$$

The channel optical path loss is given by $H(0) = \int_{-\infty}^{\infty} h(t)\,dt$, so the average received power is $P = H(0)P_t$ and the

electrical SNR at a bit rate R_b is

$$\mathrm{SNR} = \frac{R^2 P^2}{R_b N_0}. \quad (3)$$

This definition of SNR facilitates comparison of optical average-power efficiency among different L-PPM orders. It is equal to $1/L$ times the usual definition of SNR (E_b/N_0). The power constraint (2) implies that for a given average optical power P_t, the receiver SNR can be improved by transmitting a waveform $X(t)$ having a high peak-to-average ratio, such as in pulse-position modulation (PPM). Compared to simple on–off keying (OOK), PPM yields a performance enhancement at the expense of increased peak power and electrical bandwidth requirements, in addition to the need for both chip and symbol synchronization.

III. MLSD OF TRELLIS-CODED PPM

The block diagram of a trellis-coded L-PPM system is shown in Fig. 1(a) and (b). The convolutional encoder converts the input bits into coded bits at rate $-(\log_2(L - 1)/\log_2 L)$. Each group of $\log_2 L$ coded bits is then mapped to a PPM waveform $p_i(t), i = 0, \cdots, L - 1$, which has duration T. Each $p_i(t)$, denoted by symbol i, includes one "chip" of unit amplitude and duration T/L, in addition to $L - 1$ chips of zero amplitude. A sequence of $p_i(t)$ forms the chip waveform $b(t)$, which is scaled by the peak optical power LP_t and

transmitted over the fixed multipath channel $h(t)$. The MLSD receiver employs a whitened-matched filter (WMF), which consists of a unit-energy continuous-time matched filter $r(t)$, whose output is sampled at rate L/T, followed by a discrete-time noise-whitening filter w_k. The WMF output sequence q_k represents a sufficient statistic for optimal detection. We may simplify the continuous-time realization of Fig. 1(a) and (b) into the discrete-equivalent model shown in Fig. 1(c). The combination of transmitter filter, channel, receiver filter, and whitening filter is described by the causal, minimum phase, discrete-time impulse response c_k. The received samples q_k are given by

$$q_k = LP_t b_k \otimes c_k + v_k = u_k + v_k \qquad (4)$$

where the noise samples v_k are i.i.d. Gaussian random variables with zero mean and variance N_0 due to our normalization of w_k. We emphasize that these noise samples v_k are independent of the signal samples u_k, in contrast to the case of a photon-counting detector for PPM, which has been treated previously.

If we view the input chip sequence $b_k \in \{0, 1\}$ as a cyclostationary PAM signal, then given the chip samples $\{q_k\}$, the optimal trellis decoder is the maximum likelihood sequence detector (MLSD), which chooses an estimate of the sequence b_k to minimize the sum over the entire reception of the per-chip branch metric $|q_k - u_k|^2$ [13]. Since the sequence b_k is cyclostationary (and not i.i.d.), however, the MLSD cannot be implemented using a chip-rate Viterbi algorithm, but can be implemented using a symbol-by-symbol Viterbi algorithm with a per-symbol branch metric given by

$$\sum_{k=0}^{L-1} |q_k - u_k|^2. \qquad (5)$$

The union bound provides an upper bound to the probability of bit error for MLSD of trellis-coded PPM.

$$\Pr[\text{bit error}] < \sum_{\{e\}} m_{\{e\}} Q\left(\frac{d_{\{e\}}}{2\sqrt{N_0}}\right) \qquad (6)$$

where we sum over all nonzero error sequences $\{e\}$ starting at time zero, that is, over all $e_k = b_k - b'_k$, where b_k and b'_k are valid PPM chip sequences allowed by the convolutional encoder. Each error sequence $\{e\}$ corresponds to $m_{\{e\}}$ bit errors and a distance $d_{\{e\}}$ given by

$$d_{\{e\}}^2 = \sum_{k=0}^{\infty} \left| \sum_{m=0}^{\infty} c_m e_{k-m} \right|^2. \qquad (7)$$

In practice, this summation is truncated after a large but finite number of terms, thus providing an approximate upper bound. At high SNR, the probability of bit error can be well approximated by only considering terms with distances at or very near the minimum distance. This near-minimum distance bound forms an approximate lower bound.

On an ISI channel, the Viterbi decoder uses a trellis with combined code and ISI states [12]. The number of decoder states for L-PPM with a rate$-(\log_2(L-1)/\log_2 L)$ code is
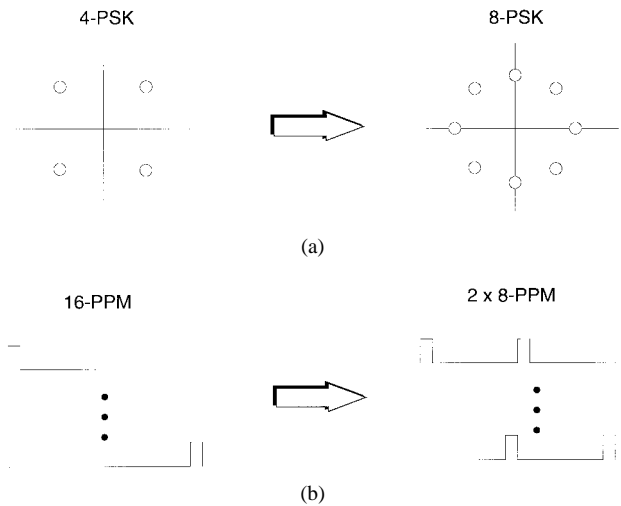

Fig. 2. Expanding the signal set to provide redundancy for coding while preserving the bandwidth: (a) PSK, (b) PPM.

$2^v (L/2)^{n_{\text{ISI}}}$, where v is the constraint length and n_{ISI} is the number of postcursor ISI symbols spanned by c_k.

IV. PERFORMANCE ON MULTIPATH ISI CHANNELS

Unequalized L-PPM suffers severe power penalties on ISI channels, particularly at high bit rates [4]. To improve the performance of L-PPM, we use trellis-coded modulation (TCM) [9], which is designed to maximize the minimum Euclidean distance between allowed signal sequences. Two key concepts of TCM are the use of signal-set expansion to provide redundancy for coding, and the use of set partitioning in code design.

For phase-shift keying (PSK), moving from 4-PSK to 8-PSK expands the signal set without increasing the bandwidth, so that a rate-2/3 code applied to 8-PSK will result in the same data rate as uncoded 4-PSK. For PPM, the corresponding analogy is to compare uncoded 16-PPM to rate-2/3-coded 8-PPM. Fig. 2 illustrates this analogy. Each 16-PPM symbol encodes four bits with a single pulse in one of 16 chips. In order to maintain the same bandwidth, the chip rate must remain constant. Suppose one transmits two pulses, each of half the original amplitude in order to maintain the same average power, with the first pulse being transmitted within the first eight chips, and the second pulse within the second eight chips. This is equivalent to two symbols of 8-PPM that encode six bits, providing a signal-set expansion with no bandwidth expansion, so that after applying a rate-2/3 code, the overall data rate is the same as uncoded 16-PPM. A similar comparison can be made between uncoded 32-PPM and rate-3/4-coded 16-PPM, although for equivalent data rates, uncoded 32-PPM has a slightly higher bandwidth.

Since PPM is an orthogonal multipulse modulation scheme, the Euclidean distance between any pair of symbols is the same on a dispersionless channel, so there is no advantage in performing set partitioning to search for good codes. However, multipath dispersion on wireless infrared channels causes symbols whose chips are adjacent in time, such as symbols
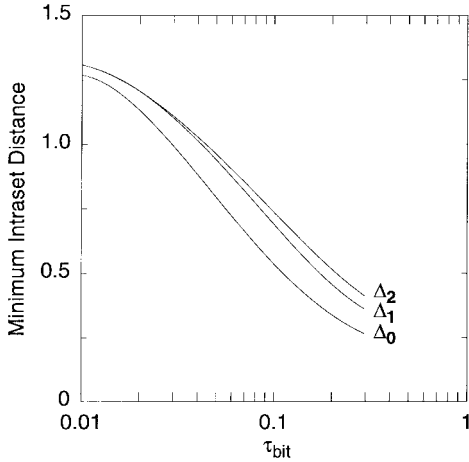
Fig. 3. Minimum Euclidean intraset distances of rate-2/3-coded, 8-PPM symbols versus τ_{bit}, the channel delay spread divided by the bit duration.
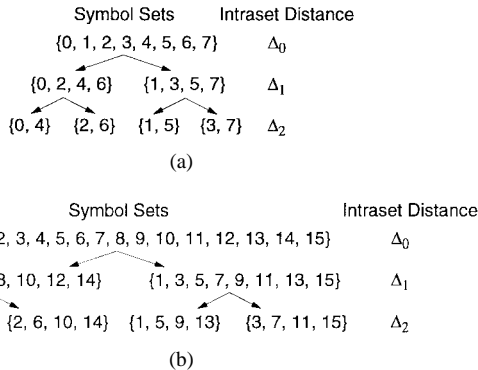

Fig. 4. Set partitioning for (a) 8-PPM and (b) 16-PPM.

0 and 1, to be separated by smaller Euclidean distances than symbols whose chips are separated in time, such as symbols 0 and 4. As the multipath-induced ISI increases, the effectiveness of a trellis code designed with set partitioning also increases.

Fig. 3 shows how the Euclidean distance between 8-PPM symbols decreases as the ISI increases. A useful measure of the impact of multipath ISI for a given channel is the channel rms delay spread, normalized by the bit duration, which we denote τ_{bit} [7]. The distances Δ_0 between symbols with adjacent chips falls quite rapidly as τ_{bit} increases, whereas the distances Δ_1 and Δ_2 between symbols with chips separated by two or four chip periods, respectively, decreases less rapidly. As the ISI increases, trellis codes designed with proper symbol mapping and set partitioning, as shown in Fig. 4, exploit these differences in distance to improve the system performance as compared to that of uncoded PPM.

Previous studies [4], [8] have used experimentally measured impulse responses of line-of-sight and diffuse channel configurations in typical offices and conference rooms. These channel responses have delay spreads of 1–10 ns, so for bit rates of 10–30 Mbits/s, we are concerned with $\tau_{\text{bit}} = 0.01$–0.3. In this study, we use channel impulse responses given by the ceiling-bounce functional model:

$$h(t) = H(0)(t+a)^{-7}u(t) \qquad (8)$$

where the rms delay spread D is

$$D(h(t,a)) = \frac{a}{12}\sqrt{\frac{13}{11}}. \qquad (9)$$

The use of the ceiling-bounce model provides a simple, highly accurate method of evaluating BER performance and average-power requirements for PPM on multipath infrared channels [11]. Moreover, it provides a standardized, reproducible method for performing code searches.

V. CODE SEARCH

Since we are interested in codes for 8-PPM and 16-PPM that work well over a range of channels with different delay spread per bit duration ratios τ_{bit}, we use a two-pass search. In the first pass, we use the code search technique in [10] to search for good codes on three channels with $\tau_{\text{bit}} = 0$, 0.06, and 0.2. We then determine the SNR required to obtain a BER of 10^{-6} for the best codes over a full suite of channels from $\tau_{\text{bit}} = 0$–0.3.

The convolutional encoder is uniquely specified by the parity-check matrix $H = (h_j^i)$. Following [10], we set $h_0^0 = h_v^0 = 1$ and $h_0^j = h_v^j = 0$, $j = 1, \cdots, \log_2 L - 1$, to guarantee at least distance Δ_1 between merging or diverging trellis transitions. Fig. 5 shows the minimal systematic encoder structure with feedback. For each of the $2^{(v-1)\log_2 L}$ codes, we evaluate the minimum distance from the all-0's path on the ideal channel $\tau_{\text{bit}} = 0$. For a constraint-length v code, the largest possible minimum distance is $\sqrt{2\lfloor v/(\log_2 L - 1)\rfloor}$ since the shortest error path is $\lfloor v/(\log_2 L - 1)\rfloor$ symbols in length and each symbol branch metric contributes either $\sqrt{2}$ or 0. This is a simple calculation that only requires counting. For codes that perform well on the ideal channel, we then compute, using the Viterbi algorithm, the minimum distance for the channels $\tau_{\text{bit}} = 0.06$ and $\tau_{\text{bit}} = 0.2$. Fig. 6 shows the WMF output of a rate-2/3-coded 8-PPM receiver from a single chip transmitted on these channels. Finally, we evaluate the SNR performance of the codes with the highest minimum distances, using a union-bound approximation of the first few dozen lowest distance error paths from the all-0's path.

Although the convolutional codes are linear, the trellis-coded PPM output is not linear, so the minimum Euclidean distance of the all-0's path is not necessarily the minimum distance of any other trellis path. For the lowest constraint-length codes $(v < 4)$, where the minimum-distance error events are short and where there is only one minimum-distance error path per trellis path, these differences in minimum distance can be significant. In these cases, in calculating the BER performance, one must average the BER given by (6) over all possible trellis paths. For a minimum distance lower bound calculation, this is feasible. For union-bound approximations, we can average over a large number of randomly selected paths.

For longer constraint-length codes, minimum-distance and union-bound approximations calculated only from the all-0's path turn out to be quite accurate. This is because there are several near-minimum-distance error paths from a given
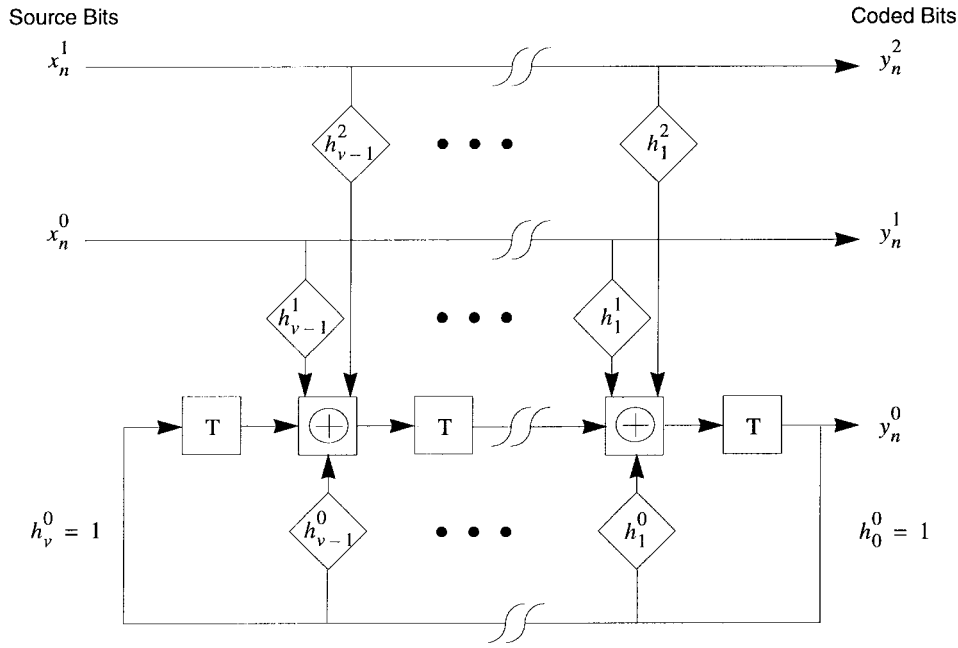
Source Bits

Coded Bits

Fig. 5.   Minimal systematic encoder with feedback for 8-PPM with parity-check coefficients h_j^i and constraint length v.
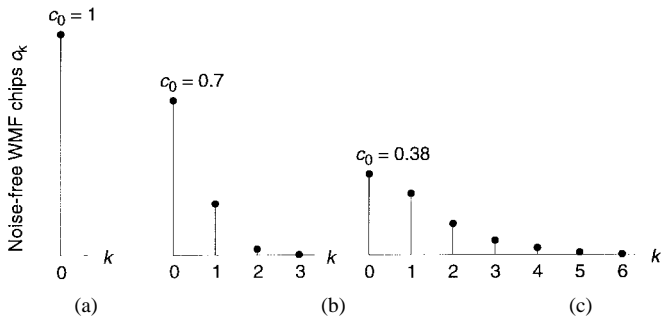
Fig. 6.   Noise-free WMF output of rate-2/3-coded 8-PPM from a single chip transmitted over the following channels: (a) $\tau_{\text{bit}} = 0$ (ideal), (b) $\tau_{\text{bit}} = 0.06$, and (c) $\tau_{\text{bit}} = 0.2$.

Fig. 7.   Normalized optical average-power requirement versus τ_{bit}, the channel delay spread divided by bit duration, for systems employing rate-2/3-coded 8-PPM, rate-3/4-coded 16-PPM, and uncoded 16-PPM and 32-PPM at 10^{-6} BER. The 0-dB optical-power reference level is OOK on the ideal channel. All curves are union-bound approximations.

transmitted path, and because the lengths of these error paths are much longer than for codes with $v < 4$. Thus, the variation among BER's calculated for different transmitted paths is quite small.

Tables I and II show the best codes for 16-PPM and 8-PPM, respectively, from this search. Parity-check elements are listed in octal form. Fig. 7 shows unionbound performance curves of these codes, as well as that of uncoded 16-PPM and 32-PPM for comparison, all evaluated at 10^{-6} BER. Trellis-coded 16-PPM has the best average-power efficiency, with gains of about 0.6 electrical dB per unit constraint-length increase for low τ_{bit}, which fall to about 0.3 electrical dB per unit constraint-length increase for high τ_{bit}. Similarly, trellis-coded 8-PPM shows gains of about 0.5 electrical dB for low τ_{bit}, which fall to about 0.3 electrical dB for high τ_{bit}. The distances Δ_0 dominate the performance of uncoded PPM, resulting in sharp rises in average-power requirements for $\tau_{\text{bit}} > 0.05$. Because of Ungerboeck's code search rules, which guarantee at least $\sqrt{2}\Delta_1$ distance between pairs of
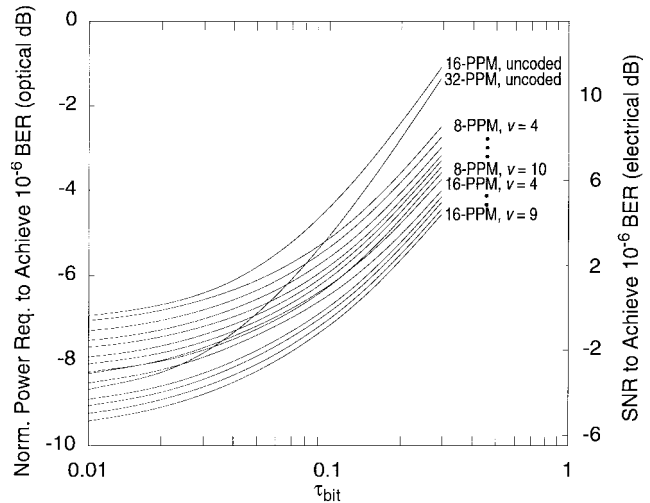
trellis paths, trellis-coded PPM performance curves have a much slower increase in average-power requirements as τ_{bit} increases. Indeed, the power requirement for trellis-coded 16-PPM with $v = 9$ is only 1.5 electrical dB lower than uncoded 32-PPM on near-ideal channels ($\tau_{\text{bit}} = 0.01$), but is 6.4 electrical dB lower on severe ISI channels ($\tau_{\text{bit}} = 0.3$). Similarly, the power requirement for trellis-coded 8-PPM with $v = 10$ is only 2.7 electrical dB lower than uncoded 16-PPM on near-ideal channels, but is 5.0 electrical dB lower on severe ISI channels.

Of course, for a given bit rate, these modulation schemes have different bandwidth requirements. Uncoded 16-PPM and

TABLE I
CODES FOR 16-PPM: PARITY-CHECK COEFFICIENTS OF THESE 16-PPM CODES ARE IN OCTAL FORM. THE NUMBER OF ERROR
PATHS WITH DISTANCE LESS THAN $d_{\min} + 0.04$ IS LISTED IN THE THREE RIGHTMOST COLUMNS. THESE ERROR PATHS HAVE
A SIGNIFICANT EFFECT AT BIT-ERROR RATES GREATER THAN 10^{-6}. SEARCH RESULTS FOR $v = 8$ AND 9 ARE INCOMPLETE

Constraint Length v	Parity-Check Coefficients				Minimum Distance d_{min} (from all-0's path)			Number of Near-minimum-distance Error Paths n_{min}		
	h^0	h^1	h^2	h^3	$\tau = 0$	$\tau = 0.06$	$\tau = 0.2$	$\tau = 0$	$\tau = 0.06$	$\tau = 0.2$
4	37	12	14	10	2.000	1.375	.8302	4	4	3
5	57	32	22	34	2.000	1.379	.8877	1	1	1
6	173	046	072	010	2.450	1.652	.9682	17	17	12
7	357	176	050	044	2.450	1.683	.9846	6	6	2
8	603	124	262	042	2.450	1.688	1.056	1	1	15
9	1211	0664	0336	0110	2.828	1.840	1.086	33	2	11

TABLE II
CODES FOR 8-PPM: PARITY-CHECK COEFFICIENTS OF THESE 8-PPM CODES ARE IN OCTAL FORM. THE NUMBER OF ERROR
PATHS WITH DISTANCE LESS THAN $d_{\min} + 0.04$ IS LISTED IN THE THREE RIGHTMOST COLUMNS. THESE ERROR PATHS HAVE A
SIGNIFICANT EFFECT AT BIT-ERROR RATES GREATER THAN 10^{-6}. SEARCH RESULTS FOR $v = 10$ ARE INCOMPLETE

Constraint Length v	Parity-Check Coefficients			Minimum Distance d_{min} (from all-0's path)			Number of Near-minimum-distance Error Paths n_{min}		
	h^0	h^1	h^2	$\tau = 0$	$\tau = 0.06$	$\tau = 0.2$	$\tau = 0$	$\tau = 0.06$	$\tau = 0.2$
4	23	16	12	2.450	1.707	.9814	5	1	1
5	43	36	14	2.450	1.809	1.092	1	1	3
6	163	056	022	2.828	2.003	1.169	10	5	3
7	203	162	104	2.828	2.076	1.260	3	3	9
8	441	376	244	3.162	2.200	1.304	15	2	10
9	1015	0736	0422	3.162	2.328	1.344	2	6	6
10	2031	1106	0422	3.464	2.411	1.367	22	5	3

trellis-coded 8-PPM have the same bandwidth requirement, but trellis-coded 16-PPM and uncoded 32-PPM require 4/3 and 8/5 higher bandwidths, respectively, in comparison. Fig. 8 provides an alternate view of the PPM performance curves, where average-power requirements are plotted against τ_{chip}, the delay spread per chip duration ratio. This figure once again shows the superiority of trellis-coded 16-PPM over the other modulation schemes.

Fig. 9 shows BER curves for the best 8-PPM and 16-PPM codes with $v = 6$ on the channel $\tau_{\mathrm{bit}} = 0.06$. It shows near-minimum-distance and union-bound curves calculated from (6), as well as Monte Carlo simulation results, which verify the accuracy of BER calculations from the all-0's path. At 10^{-5} BER, the two bounds both narrow to within 0.1 and 0.2 electrical dB from the simulation curve for 8-PPM and 16-PPM, respectively, thus providing very accurate estimates of the BER performance.

VI. CONCLUSIONS

Trellis-coded pulse-position modulation (PPM) is a promising method for high-speed wireless indoor infrared communications. We presented a detailed performance assessment of the
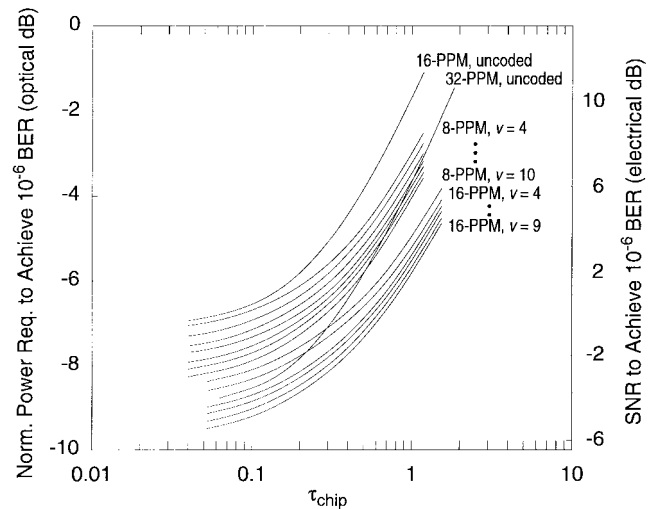

Fig. 8. Normalized optical average-power requirement versus τ_{chip}, the channel delay spread divided by chip duration, for systems employing rate-2/3-coded 8-PPM, rate-3/4-coded 16-PPM, and uncoded 16-PPM and 32-PPM at 10^{-6} BER. The 0-dB optical-power reference level is OOK on the ideal channel. All curves are union-bound approximations.

MLSD of rate-2/3-coded 8-PPM and rate-3/4-coded 16-PPM on multipath channels that demonstrates the effectiveness of
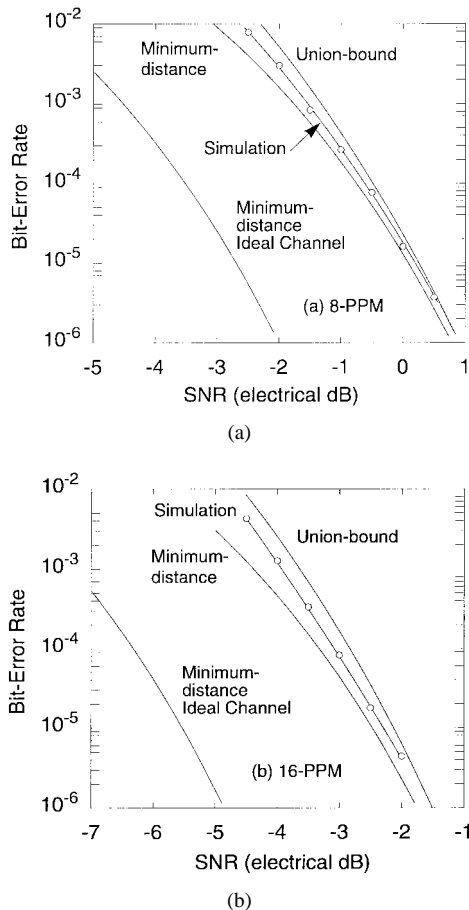
Fig. 9. BER performance curves for (a) 8-PPM and (b) 16-PPM, constraint length $v = 6$ codes from Tables I and II. Near-minimum distance, union-bound, and Monte Carlo simulation curves are shown for $\tau_{\mathrm{bit}} = 0.06$, with a minimum-distance curve for $\tau_{\mathrm{bit}} = 0$ (ideal channel) to show the ISI penalty.

trelis coding at minimizing the effects of multipath-induced intersymbol interference. We also listed high-constraint-length codes found using Ungerboeck's search technique [10]. Finally, we provided Monte Carlo simulation results to verify the accuracy of our analysis. Our results indicate that rate-3/4-coded 16-PPM has the highest average-power efficiency, with gains of up to 6.3 electrical dB over uncoded 32-PPM for a constraint-length-9 code, even though it has a slightly lower bandwidth requirement. Similarly, rate-2/3-coded 8-PPM has gains of up to 5.0 electrical dB over uncoded 16-PPM for a constraint-length-10 code, even though both have the same bandwidth requirement.

REFERENCES

[1] F. R. Gfeller and U. H. Bapst, "Wireless in-house data communication via diffuse infrared radiation," *Proc. IEEE*, vol. 67, pp. 1474–1486, Nov. 1979.
[2] J. M. Kahn, J. R. Barry, M. D. Audeh, J. B. Carruthers, W. J. Krause, and G. W. Marsh, "Non-directed infrared links for high-capacity wireless LAN's," *IEEE Personal Commun. Mag.*, vol. 1, pp. 12–25, Spring 1994.
[3] J. R. Barry, *Wireless Infrared Communications*. Boston, MA: Kluwer Academic, 1994.
[4] M. D. Audeh, J. M. Kahn, and J. R. Barry, "Performance of pulse-position modulation on measured non-directed indoor infrared channels," *IEEE Trans. Commun.*, vol. 44, pp. 654–659, June 1996.
[5] E. Forestieri, R. Gangopadhyay, and G. Prati, "Performance of convolutional codes in a direct-detection optical PPM channel," *IEEE Trans. Commun.*, vol. 37, pp. 1303–1317, Dec. 1989.
[6] G. Prati and R. Gagliardi, "Block encoding and decoding for the optical PPM channel," *IEEE Trans. Inform. Theory*, vol. IT-28, pp. 100–105, Jan. 1982.
[7] J. M. Kahn, W. J. Krause, and J. B. Carruthers, "Experimental characterization of non-directed indoor infrared channels," *IEEE Trans. Commun.*, vol. 43, pp. 1613–1623, Feb./Mar./Apr. 1995.
[8] D. C. Lee, J. M. Kahn, and M. D. Audeh, "Performance of pulse-position modulation with trellis-coded modulation on non-directed indoor infrared channels," in *Proc. IEEE GLOBECOM'95*, vol. 3, Singapore, Nov. 1995, pp. 1830–1834.
[9] G. Ungerboeck, "Trellis-coded modulation with redundant signal sets, Part I: Introduction," *IEEE Commun. Mag.*, vol. 25, pp. 5–11, Feb. 1987.
[10] ——, "Trellis-coded modulation with redundant signal sets, Part II: State of the art," *IEEE Commun. Mag.*, vol. 25, pp. 12–21, Feb. 1987.
[11] J. B. Carruthers and J. M. Kahn, "Modeling of non-directed wireless infrared channels," in *Proc. IEEE Int. Conf. Commun. (ICC'96)*, Dallas, TX, June 1996. Also, *IEEE Trans Commun.*, to be published.
[12] P. R. Chevillat and E. Eleftheriou, "Decoding of trellis-encoded signals in the presence of intersymbol interference," *IEEE Trans. Commun.*, vol. 37, pp. 669–676, July 1989.
[13] J. R. Barry, "Sequence detection and equalization for pulse-position modulation," in *Proc. IEEE Int. Conf. Commun.*, New Orleans, LA, May 1994, pp. 1561–1565.

David C. M. Lee (S'88) received the B.Sc. degree (Hons.) in mathematics and the B.E. degree in electrical engineering from the University of Saskatchewan, Saskatoon, Sask., Canada, in 1993. He is currently pursuing the Ph.D. degree in the Department of Electrical Engineering and Computer Sciences, University of California, Berkeley, specializing in indoor wireless infrared communications.

Mr. Lee's studies and research have been supported by an Office of Naval Research Graduate Fellowship and a Natural Sciences and Engineering Research Council of Canada Scholarship.

Joseph M. Kahn (M'87) received the A.B., M.A. and Ph.D. degrees in physics from the University of California, Berkeley in 1981, 1983 and 1986, respectively. His Ph.D. dissertation was entitled "Hydrogen-Related Acceptor Complexes in Germanium".

From 1987 to 1990 he was a Member of Technical Staff in the Lightwave Communications Research Department of AT&T Bell Laboratories, Crawford Hill Laboratory, Holmdel, NJ, where he performed research on multi-gigabit-per-second coherent optical fiber transmission systems and related device and subsystem technologies. He demonstrated the first BPSK-homodyne optical fiber transmission system, and achieved world records for receiver sensitivity in multi-gigabit-per-second systems. He joined the faculty of UC-Berkeley in 1990, where he is a Professor in the Department of Electrical Engineering and Computer Sciences. His research interests include infrared and radio wireless communications, and optical fiber communications.

Dr. Kahn is a recipient of the National Science Foundation Presidential Young Investigator Award, and is a member of the IEEE Communications Society and IEEE Lasers and Electro-Optics Society. He is serving currently as a technical editor of *IEEE Personal Communications Magazine*.

Malik D. Audeh (S'87–M'95) was born in Huntsville, AL, in May 1968. He received the B.S. degree in electrical engineering with highest honors in 1990 from the University of Illinois at Urbana-Champaign, and the M.S. and Ph.D. degrees in electrical engineering in 1992 and 1995, respectively, from the University of California, Berkeley.

Since 1995, he has been a Principal Member of Technical Staff at Telesis Technologies Laboratory, San Ramon, CA. His current research interests are multichannel multipoint distribution services (MMDS), infrared and radio-based wireless local communications, and broadband wireless communication systems.